

Cite this: *Soft Matter*, 2011, **7**, 3491

www.rsc.org/softmatter

PAPER

## Ionic liquid crystals derived from 4-hydroxypyridine†

Jung-Tang Lu, Ching-Kuan Lee and Ivan J. B. Lin\*

Received 25th November 2010, Accepted 5th January 2011

DOI: 10.1039/c0sm01376e

Monoalkylation of 4-hydroxypyridine gave either neutral *N*-alkyl-4-pyridones or 4-alkoxy-pyridines depending on the site (N or O) of alkylation. Further alkylation of these two neutral compounds yielded ionic liquid crystals (ILCs) of *N*-alkyl-4-alkoxy-pyridinium bromide, having two long alkyl chains. Alternatively, simple protonation of the two neutral compounds with HCl also induced the formation of ILCs of *N*-alkyl-4-hydroxypyridinium chloride or 4-alkoxy-pyridinium hydrochloride. Crystal structures of two different types of ionic liquid crystals and one neutral compound were determined *via* single crystal X-ray diffraction. Mesophase properties were examined by the technique of differential scanning calorimetry, polarized optical microscopy, and powder X-ray diffractometry. Anions influence the structure and stability of the mesophase in the dialkylated compounds. The self-assembly behavior of some typical compounds in solution was studied using the technique of NMR diffusion order spectroscopy. Finally, stable Au nanoparticles stabilized by a pyridinium salt were prepared and characterized.

### Introduction

Ionic liquid crystals (ILCs)<sup>1</sup> are amphiphiles and are special type of ionic liquids (ILs).<sup>2</sup> ILs are a new generation of green solvent, having low vapor pressure, high polarity and tunable compatibility towards various solvents. ILCs, having either positively or negatively charged ionic head groups tend to assemble so as to provide partially ordered environments through Coulombic, hydrophobic, dipole–dipole and hydrogen bonding interactions, and usually form a lamellar mesophase. Recent developments show that cationic amphiphiles have many interesting properties and have been used as templating and protecting agents for nanoparticle formation,<sup>3</sup> gelators,<sup>4</sup> ionic conductors,<sup>5</sup> surfactants,<sup>6</sup> ionic liquids,<sup>7</sup> and anti-bacterial agents.<sup>8</sup> The most widely studied systems of ILCs include ammonium,<sup>9</sup> phosphonium,<sup>10</sup> imidazolium,<sup>11</sup> pyrrolidinium<sup>12</sup> and pyridinium salts.<sup>11a–b,13</sup> Our group have been working on imidazolium based ILCs,<sup>14</sup> and now wish to extend our study to ILCs of pyridinium salts. Most of the known pyridinium based ILCs are salts with only one alkyl chain. Liquid crystals of pyridinium salts with two long alkyl chains are rare; for example, protonation of pyridine with two alkyl chains at the 2 and 6 positions produces pyridinium LCs;<sup>13f</sup> another example has an *N*-alkyl chain and an oxadiazole group at the 4-position of the pyridine ring.<sup>13g</sup>

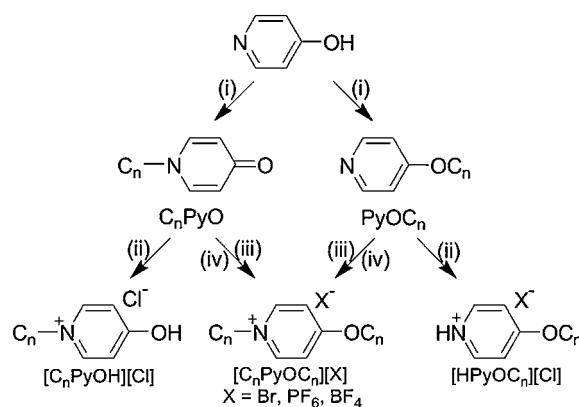
In this work we chose 4-hydroxypyridine as our starting material to prepare pyridinium salts. Monoalkylation of 4-hydroxypyridine could produce *N*-substituted pyridones or

*O*-substituted pyridines (Scheme 1). These *N*- or *O*-substituted products could further react with alkyl halide to produce *N*-alkyl-4-alkoxy-pyridinium salts, or react with hydrochloric acid to give *N*-alkyl-4-hydroxypyridinium and *N*-*H*-4-alkoxy-pyridinium salts. We study their assembly behaviors in solution, solid, and the mesophase. A pyridinium salt was also used as a protecting ligand, to fabricate the gold nanoparticles.

### Results and discussion

#### Synthesis

***N*-Alkyl-4-pyridones.** This series of compounds ( $C_n\text{PyO}$ ,  $C_n$  stands for  $C_nH_{2n+1}$ ,  $n = 12, 14, 16$  and  $18$ ), a type of zwitterion, were produced through a slight modification of a known reaction.<sup>15</sup> Addition of a phase transfer agent, tetrabutylammonium



**Scheme 1** (i)  $C_nH_{2n+1}Br$ , 2N NaOH, TBAB, THF, reflux, 24 h; (ii) HCl (conc.),  $CH_3OH$ , RT, 2 h; (iii)  $C_nH_{2n+1}Br$ , 85 °C, 24 h; (iv) after (iii),  $NH_4X$  ( $X = BF_4, PF_6$ ), ethanol, RT, 2 h.

Department of Chemistry, National Dong-Hwa University, Shoufeng, Hualien, 974, Taiwan. E-mail: [ijblin@mail.ndhu.edu.tw](mailto:ijblin@mail.ndhu.edu.tw); Fax: +886-3-863-3570; Tel: +886-3-863-3599

† Electronic supplementary information (ESI) available: The crystal data, NMR and IR spectra are provided in the electronic supporting information. CCDC reference numbers [802278–802280]. For ESI and crystallographic data in CIF or other electronic format see DOI: 10.1039/c0sm01376e

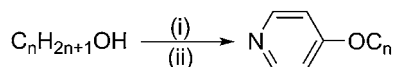
bromide (TBAB), improves the yields substantially (Scheme 1). In our hands, an increase in the yields from 30–40% to 70–80% was observed. Although isomerization of an *O*-arylated product to an *N*-arylated product had been claimed to be a part of the reasons for the preferential formation of an *N*-substituted product,<sup>15b</sup> such isomerization did not occur in our case, as monitored by <sup>1</sup>H-NMR spectroscopy.

**4-Alkoxyppyridines.** Several approaches are known for the preparation of the title compounds. Attempts to produce 4-alkoxyppyridine (PyOC<sub>*n*</sub>, *n* = 12, 14, 16 and 18) *via* direct alkylation of 4-hydroxyppyridine results in low product yields. Two other synthesis methods are known for 4-alkoxylated products.<sup>16,17</sup> With slight modification, the method described in ref. 18 was used. In this work, long chain alcohols were heated in DMSO with NaOH at 100 °C for 1 h, then 4-chloropyridine was added and reacted for 24 h to produce 4-alkoxylated products (Scheme 2).

**Pyridinium salts.** The preparation of *N*- and 4-disubstituted pyridinium salts are schematically represented in Scheme 1. *N*-Alkyl-4-alkoxyppyridinium bromides (denoted as [C<sub>*n*</sub>PyOC<sub>*n*</sub>][Br], *n* = 10, 12, 14, 16 and 18) were synthesized by the reaction of either *N*-alkyl-4-pyridones or 4-alkoxyppyridines with alkyl bromide at 80 °C. Metathesis of the bromide salts by ammonium hexafluorophosphate (NH<sub>4</sub>PF<sub>6</sub>) and ammonium tetrafluoroborate (NH<sub>4</sub>BF<sub>4</sub>) produced *N*-alkyl-4-alkoxyppyridinium hexafluorophosphate ([C<sub>*n*</sub>PyOC<sub>*n*</sub>][PF<sub>6</sub>], *n* = 10, 12, 14, 16 and 18) and *N*-alkyl-4-alkoxyppyridinium tetrafluoroborate ([C<sub>*n*</sub>PyOC<sub>*n*</sub>][BF<sub>4</sub>], *n* = 10, 12, 14, 16 and 18), respectively. *N*-Alkyl-4-hydroxyppyridinium chlorides ([C<sub>*n*</sub>PyOH][Cl], *n* = 12, 14, 16 and 18) and 4-alkoxyppyridinium hydrochlorides ([HPyOC<sub>*n*</sub>][Cl], *n* = 12, 14, 16 and 18) were obtained through direct protonation of *N*-alkyl-4-pyridones and 4-alkoxyppyridines with concentrated HCl.

### Crystal structure

**[C<sub>16</sub>PyO]·H<sub>2</sub>O.** Crystals of this compound suitable for single crystal X-ray diffraction were obtained from the CH<sub>2</sub>Cl<sub>2</sub>/hexane solvent system. The source of the hydrate is from the trace of water in the non-treated solvent. The crystal data are given in ESI (Table S1-S2),† and an ORTEP drawing in Fig. 1(a). The C(3)–O(1) bond length of 1.270(3) Å is comparable to the known pyridone CO bond length (1.274(6) Å).<sup>18</sup> For reference, the C=O double bond is 1.20 Å, and C–O single bond is about 1.33 Å.<sup>19</sup> The N(1)–C(1) (1.335(3) Å) and N(1)–C(5) (1.339(3) Å) bonds are *ca.* 0.02 Å longer than the corresponding N–C bonds in 4-hydroxyppyridine (1.319 Å); while the C(1)–C(2) (1.352(3) Å) and C(4)–C(5) (1.352(3) Å) bonds are *ca.* 0.03 Å shorter than those of the corresponding C–C bonds found in 4-hydroxyppyridine (1.384 Å). Consequently, the nature of this compound is a resonance hybrid of the dearomatized *N*-alkyl-4-pyridone and the



**Scheme 2** (i) Excess of NaOH, DMSO, 100 °C, 1 h; (ii) 4-chloropyridine, 100 °C, 24 h.

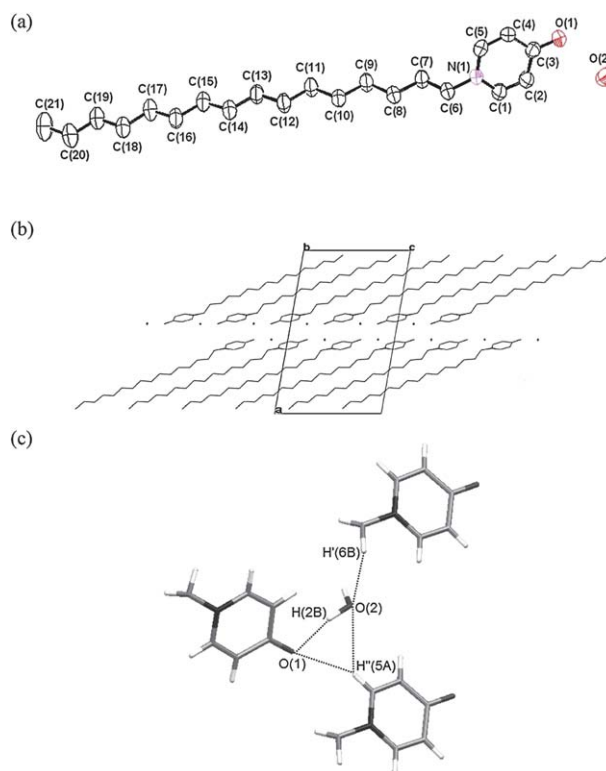


**Fig. 1** (a) Perspective view and atomic labeling for the compound [C<sub>16</sub>PyO]·H<sub>2</sub>O; thermal ellipsoids are set at 50%. Hydrogens are omitted for clarity. Selected bond lengths [Å] and angles [°]: O(1)–C(3) 1.270(3); N(1)–C(1) 1.335(3); N(1)–C(5) 1.339(3); N(1)–C(6) 1.479(3); C(1)–C(2) 1.352(3); O(4)–C(5) 1.352(3); C(1)–N(1)–C(5) 118.3(2); C(5)–N(1)–C(6) 120.2(2); O(1)–C(3)–C(2) 123.2(3); N(1)–C(6)–C(7) 115.3(2). (b) Crystal packing of [C<sub>16</sub>PyO]·H<sub>2</sub>O viewed down the *b*-axis. (c) H-bonding interactions between H<sub>2</sub>O and pyridones (Å): H''(5A)···O(2) 2.615; H'(6B)···O(2) 2.676; H(2B)···O(1) 1.917; H''(5A)···O(1) 2.575. Atoms with prime (') label are at (*x*, 1/2 – *y*, –1/2 + *z*) and the double prime (") label at (*x*, 1.5 – *y*, –1/2 + *z*).

zwitterion (Scheme 3). The alkyl chain stretches outward at a tilting angle of *ca.* 30° from the plane extended from the pyridine ring. The molecules are packed in a non-interdigitated bilayer fashion and the molecular rods tilt *ca.* 68° from the normal of the layer plane (*a*–*c* plane) (Fig. 1(b)). Extended hydrogen bonding interactions are observed among pyridones and the hydrate water: H''(5A)···O(1) (2.575 Å), H'(6B)···O(2) (2.676 Å), H''(5A)···O(2) (2.615 Å) and H(2B)···O(1) (1.917 Å) (Fig. 1(c)).

**[C<sub>16</sub>PyOC<sub>16</sub>][Br]·H<sub>2</sub>O.** Crystals of this compound were obtained from the CH<sub>2</sub>Cl<sub>2</sub>/ether solvent system. The crystal data is shown in ESI (Table S3-S4),† and the rod-like structure is drawn in Fig. 2(a). The bond lengths and angles of this compound are normal. The *N*-alkyl and -alkoxy chains stretch in opposite directions and tilt *ca.* 39° and 48° from the extended



**Scheme 3**

pyridinium ring plane, respectively. This compound has a molecular length of *ca.* 42.7 Å, and packs in a non-interdigitated monolayer fashion (Fig. 2(b)). Hydrogen bonding interactions are formed among bromide, H<sub>2</sub>O and pyridinium cations: H(1A)...Br(1) (2.743 Å), H(2A)...Br(1) (2.521 Å), H''(2B)...Br(1) (2.598 Å), H(6A)...Br''(1) (2.865 Å), H'(5A)...Br''(1) (2.809 Å), H(2C)...O(2) (2.452 Å) and H'(4A)...O''(2) (2.344 Å) (Fig. 2(c)). One can consider two pyridinium salts as a pair, in which the two pyridinium cores are associated in a head to tail fashion *via* hydrogen bondings as described above, and the  $\pi$ - $\pi$  interactions with a distance of 3.4 Å (Fig. 2(d)). Tilting of the molecular rod *ca.* 45° from the normal of the layer plane gives a layer distance of 33.4 Å. In general, an alkyl chain favors a staggered conformation and adopts a zigzag fashion, as is observed between C(22) and C(37). The “*gauche* conformation” observed at the alkyl chain next to the oxygen atom is probably due to the favorable intramolecular hydrogen bonding between H(8B) and O(1) (2.636 Å), and maximizing the hydrophobic interactions in the crystal packing.

**[C<sub>16</sub>PyOH][Cl]·H<sub>2</sub>O.** Crystals were obtained from the CH<sub>2</sub>Cl<sub>2</sub>/hexane solvent system. The crystal data is given in the

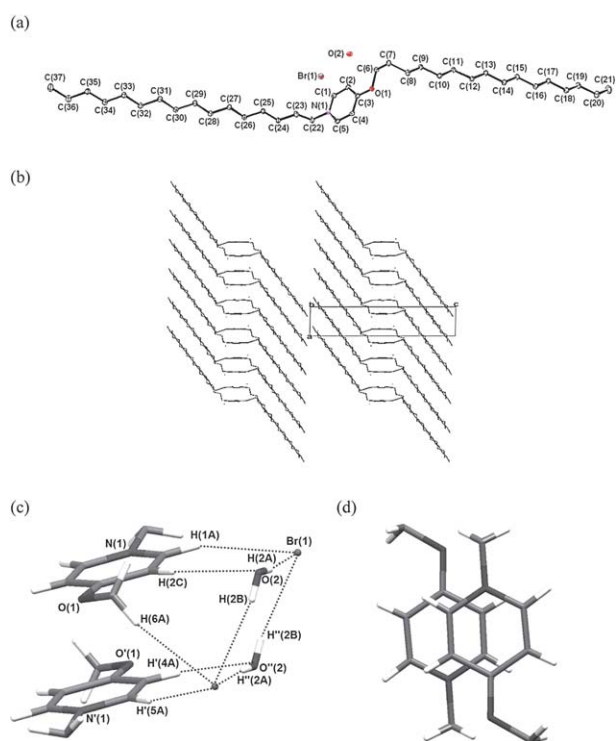


**Fig. 2** (a) Perspective view and atom labeling of compound [C<sub>16</sub>PyOC<sub>16</sub>][Br]·H<sub>2</sub>O; H atoms omitted for clarity. Selected bond lengths [Å] and angles [°]: O(1)–C(3) 1.335(2); O(1)–C(6) 1.467(2); N(1)–C(22) 1.491(2); C(1)–C(2) 1.376(3); C(4)–C(5) 1.366(3); C(3)–O(1)–C(6) 118.4(2); C(1)–N(1)–C(5) 119.7(2); O(1)–C(6)–C(7) 107.3(2); N(1)–C(22)–C(23) 109.2(2). (b) Crystal packing of [C<sub>16</sub>PyOC<sub>16</sub>][Br]·H<sub>2</sub>O viewed down the *b*-axis. (c) H-bonding interactions between the H<sub>2</sub>O, anion and cation (Å): H(1A)...Br(1) 2.743; H(2A)...Br(1) 2.521; H''(2B)...Br(1) 2.598; H(6A)...Br''(1) 2.865; H'(5A)...Br''(1) 2.809; H(2C)...O(2) 2.452; H'(4A)...O''(2) 2.344. The additional symbols of (') and (') indicate that these atoms are at (1 – *x*, –1 – *y*, 1 – *z*) and (1 – *x*, –*y*, 1 – *z*). (d) The  $\pi$ - $\pi$  interaction of 3.4 Å between pyridinium rings.

ESI (Table S5-S6),† and the molecular structure is shown in Fig. 3(a). The alkyl chain extends at a tilting angle of *ca.* 32° from the pyridinium ring plane. This compound has normal bond angles and lengths compared with those found in the pyridinium salts.<sup>13d-e</sup> The molecular cation has a structure similar to that of [C<sub>16</sub>PyOC<sub>16</sub>][Br]·H<sub>2</sub>O. The packing diagram shows that these molecules are stacked in an interdigitated bilayer fashion (Fig. 3(b)) with a repeating layer distance of *ca.* 29.5 Å. Hydrogen bonding interactions are formed among hydrated water, chloride and pyridinium moieties: H(3)...Cl(1) (2.653 Å), H'(4)...Cl(1) (2.874 Å), H'(1A)...Cl(1) (2.155 Å), H''(1)...O(1) (2.595 Å), H(2)...O'''(2) (2.539 Å), H\*(20B)...O'''(2) (2.590 Å) (Fig. 3(c)). Hydrogen bonding interactions between the pyridinium cores are the cause of their LC phase formation.

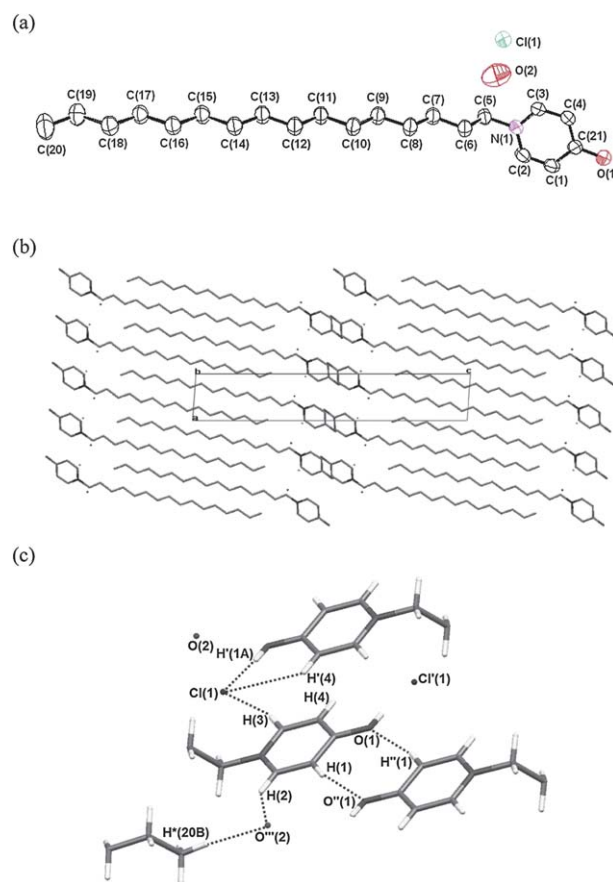


**Fig. 3** (a) Perspective view and atomic labeling of compound [C<sub>16</sub>PyOH][Cl]·H<sub>2</sub>O; H atoms are omitted for clarity; thermal ellipsoids are set at 50%. Selected bond lengths [Å] and angles [°]: O(1)–C(21) 1.328(2); N(1)–C(5) 1.482(2); C(1)–C(2) 1.366(3); C(3)–C(4) 1.360(3); O(1)–C(21)–C(4) 123.1(2); C(3)–N(1)–C(2) 119.4(2); N(1)–C(5)–C(6) 113.5(2). (b) Crystal packing of [C<sub>16</sub>PyOH][Cl]·H<sub>2</sub>O viewed down the *b*-axis. (c) H-bonding interactions between H<sub>2</sub>O, chloride and cations (Å): H(3)...Cl(1) 2.653; H'(4)...Cl(1) 2.874; H'(1A)...Cl(1) 2.155; H''(1)...O(1) 2.595; H(2)...O'''(2) 2.539; H\*(20B)...O'''(2) 2.590. The additional symbols of ('), ('), (') and (\*) indicate that these atoms are at (1 – *x*, 2 – *y*, 1 – *z*), (3 – *x*, 3 – *y*, 1 – *z*), (1 + *x*, 1 + *y*, *z*) and (1 – *x*, 2 – *y*, –*z*), respectively.

## Liquid crystalline properties

Liquid crystalline behaviors of the pyridinium salts were studied by polarized optical microscopy (POM), differential scanning calorimetry (DSC) and powder X-ray diffraction (PXRD). In all cases, SmA mesophases are detected. To avoid the influence of H<sub>2</sub>O on the thermal behavior in the process of DSC measurements, the hydrated samples were heated at 100 °C for 1 h on the sample holder, in which the cover of the cell lid was punched with a hole to allow the evaporation of water. The phase transitions and thermodynamic data of these ionic liquid crystals are shown in Table 1. The layer distances of these compounds at different phases and temperatures are given in Table 2. The neutral compounds, [C<sub>n</sub>PyO] and [PyOC<sub>n</sub>] are non-mesomorphic.

The POM image of [C<sub>n</sub>PyOC<sub>n</sub>][Br] shows that upon melting, the fluid exhibits focal-conic texture and homeotropic domain, the latter is caused by the alignment of the molecular vector orthogonal to the substrate but parallel to the light source, a typical behavior for the SmA mesophase. The DSC thermogram for the compound with *n* = 18 shows that the phase transition from the crystal to the mesophase appears at 86.9 °C with an enthalpy of 73.7 kJ mol<sup>-1</sup>, and the transition to an isotropic liquid appears at 132.9 °C with an enthalpy of 1.7 kJ mol<sup>-1</sup>. The small enthalpy value upon clearing is consistent with the existence of the mesophase. The compounds of *n* = 16, 14, 12 and 10 have melting temperatures at 78.5, 76.9, 69.6 and 62.8 °C and clearing temperatures at 133.3, 135.5, 120.2 and 69.3 °C, respectively. The chain length has a minimum influence on the clearing process for *n* = 18, 16 and 14, suggesting Coulombic, hydrogen bonding and dipole, but not hydrophobic, interactions are dominating in this process. These salts have a mesophase temperature range of Δ*T* of about 55 °C, except for *n* = 10, which has a Δ*T* value of 6.5 °C. It appears that the hydrophobic interactions arising from the ten-carbon chain length is barely large enough to sustain the formation of the mesophase for the compound where *n* = 10.

PXRD was utilized to characterize the mesophase structures. Since single crystal structural data of [C<sub>16</sub>PyOC<sub>16</sub>][Br] is available, results of this compound will be discussed first. The solid sample shows a set of three equally spaced peaks at small angle regions corresponding to (001), (002) and (003) reflections, suggesting a well-defined lamellar structure with a layer distance of 33.2 Å, consistent with that from single crystal results (Fig. 4). If the temperature is raised to a mesophase at 90 °C, the layer spacing increases slightly to 34.4 Å and a faint halo at medium angle is observed. Upon further heating to 100 and 110 °C, the layer distance decreases gradually to 33.8 and 32.9 Å. The slight increase of layer distance from the crystal to the mesophase is presumably caused by the alignment of the molecular rod perpendicular to the layer plane, which tends to elongate the layer spacing, and at the same time thermal motion of the chains at the mesophase tends to shorten the layer spacing (Scheme 4). These results are consistent with an SmA mesophase. Similar arguments apply to the other members in the bromide series.

The PF<sub>6</sub><sup>-</sup> series compound of *n* = 10 is non-mesomorphic. For the other members, fan and homeotropic textures are observed under POM, again suggesting a SmA mesophase (Fig. 5 for *n* = 16). For the compound of *n* = 18, the DSC thermogram shows that the melting process from crystal to mesophase occurs at

83.7 °C, and the clearing process occurs at 129.0 °C. Compounds of *n* = 16 and 14 have a similar phase transition behavior to that of *n* = 18, but for *n* = 12, the mesophase is observed only in the cooling process. For *n* = 10, only a simple melting process occurs at 37.9 °C and due to severe super-cooling, the freezing process does not occur above 0 °C; it thus behaves as a room temperature ionic liquid. The chain length influences both the melting and clearing processes; this is especially true when comparing to the clearing temperature of the bromide salts of *n* = 18, 16 and 14. All the above results suggest a weaker cation–anion interaction for the PF<sub>6</sub><sup>-</sup> than for the Br<sup>-</sup>. The PF<sub>6</sub><sup>-</sup> anion also causes a smaller mesophase range in this series. Interestingly, the diffractogram shows that in the solid state the layer distance of 23.9 Å for the PF<sub>6</sub><sup>-</sup> salt of *n* = 16 is 9.3 Å shorter than the corresponding bromide salt. It is likely that the larger anion allows the carbon chains to interdigitate to have more efficient packing. Upon heating to 90 °C, above the melting point, the layer distance increases from 23.9 Å in the solid state to 29.0 Å in the mesophase; the latter is *ca.* 5 Å shorter than the non-interdigitated Br<sup>-</sup> analogue suggesting a partially interdigitated alkyl chain in the mesophase. Upon increasing the temperature further to 100 and 110 °C in the mesophase, there is a slight decrease in the layer distance (28.8 and 28.6 Å respectively), again consistent with a SmA mesophase. A similar change of layer distance from the solid to the mesophase was observed for the compounds of *n* = 18 and 14.

For the BF<sub>4</sub><sup>-</sup> series, similar textures are observed in the mesophase as for the Br<sup>-</sup> and PF<sub>6</sub><sup>-</sup> series. DSC thermograms show that for the compounds of *n* = 18, 16, 14 and 12, the melting processes occur at 69.8, 63.0, 51.2 and 39.4 °C and the clearing processes appear at 127.9, 113.5, 98.2 and 77.3 °C respectively. For *n* = 10, only a simple melting process is observed at 46.8 °C. At room temperature, these BF<sub>4</sub><sup>-</sup> compounds have slightly longer layer spacings (*ca.* 2–3 Å) than the PF<sub>6</sub><sup>-</sup> compounds, but are substantially shorter (*ca.* 6–8 Å) than the corresponding Br<sup>-</sup> series. An interdigitated monolayer packing with a smaller tilting angle from the normal plane than the PF<sub>6</sub><sup>-</sup> salts is proposed for the solid structure. In the mesophase, a lamellar structure with layer spacings very similar to the PF<sub>6</sub><sup>-</sup> salts but much shorter (up to *ca.* 5 Å) than the Br<sup>-</sup> analogues are also observed, thus a partially interdigitated chain is proposed.

Among the [C<sub>n</sub>PyOH][Cl] compounds (*n* = 18, 16, 14 and 12), only *n* = 18 and 16 exhibit liquid crystalline properties with the SmA mesophase as evidenced by the textures observed under POM and results of DSC and PXRD studies. The melting temperatures for compounds of *n* = 18 and 16 are at 87.0 and 84.5 °C, respectively, and clearing temperatures are 157.1 and 114.9 °C, respectively. As revealed by the single crystal structure for the compound of *n* = 16, an interdigitated bilayer stacking with molecular rods tilting 15° from the layer plane gives a layer distance of 29.5 Å. Upon heating to 90 °C in the mesophase, a slight elongation of layer distance to 31.7 Å is observed. This result suggests a partially interdigitated lamellar mesophase (Scheme 5).

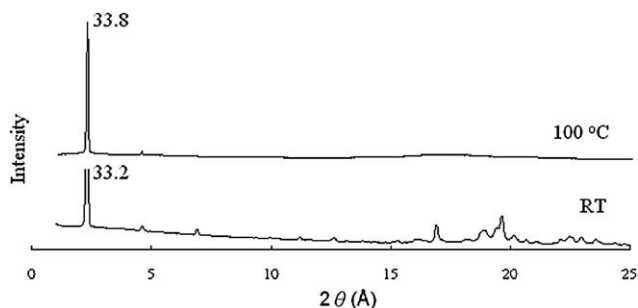
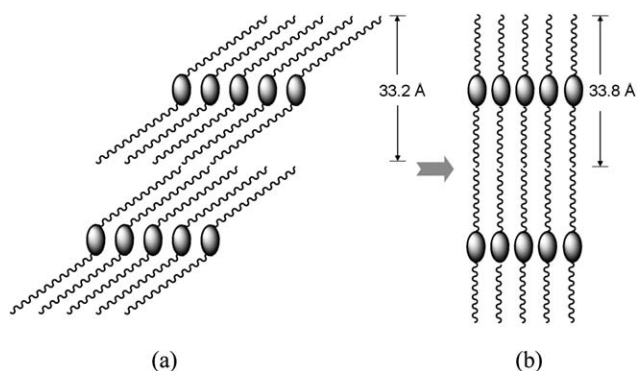
All the [HPyOC<sub>n</sub>][Cl] compounds (*n* = 18, 16, 14 and 12) exhibit liquid crystalline properties similar to the SmA mesophase. DSC thermograms reveal that the melting temperatures are at 124.0, 124.2, 122.4 and 121.8 °C for compounds of *n* = 18 to 12, respectively. The corresponding clearing temperatures are

**Table 1** Phase transition temperatures (°C) and corresponding enthalpies (kJ mol<sup>-1</sup>), in parentheses, for the pyridinium salts (Cr = crystal; Cr\* = other crystal; SmA = smectic A; I = isotropic and n. d. means the phase temperature transition by polarized optical microscope).

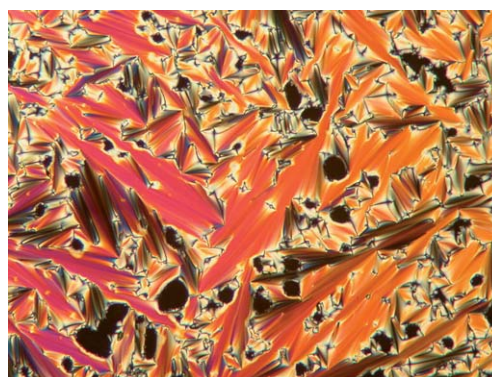
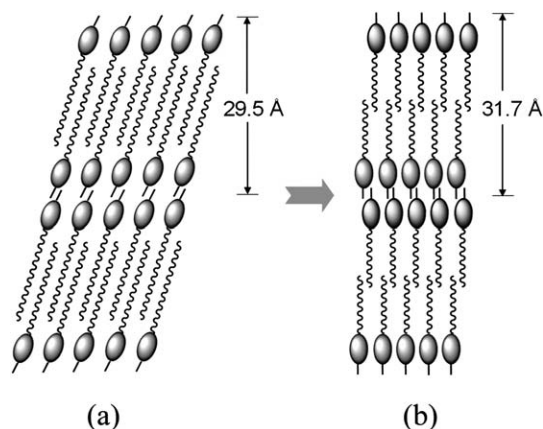
[C <sub>n</sub> PyOC <sub>n</sub> ][Br]	n = 18	Cr	$\xrightarrow{86.9 (73.7)}$	SmA	$\xrightarrow{132.9 (1.7)}$	I		
					$\xleftarrow{74.2 (65.8)}$			
	16	Cr	$\xrightarrow{78.5 (94.4)}$	SmA	$\xrightarrow{133.3 (2.3)}$	I		
					$\xleftarrow{34.6 (52.5)}$			
	14	Cr	$\xrightarrow{76.9 (64.0)}$	Cr*	$\xrightarrow{42.1 (41.6)}$	SmA	$\xrightarrow{135.5 (2.4)}$	I
					$\xleftarrow{18.7 (10.7)}$			
	12	Cr	$\xrightarrow{69.6 (55.6)}$	Cr*	$\xrightarrow{32.6 (34.5)}$	SmA	$\xrightarrow{120.2 (2.3)}$	I
						$\xleftarrow{21.3 (4.7)}$		
	10	Cr	$\xrightarrow{62.8 (41.9)}$			SmA	$\xrightarrow{69.3 (1.3)}$	I
						$\xleftarrow{40.5 (37.3)}$		
[C <sub>n</sub> PyOC <sub>n</sub> ][PF <sub>6</sub> ]	n = 18	Cr	$\xrightarrow{83.7 (110.3)}$			SmA	$\xrightarrow{129.0 (2.5)}$	I
						$\xleftarrow{60.0 (70.1)}$		
	16	Cr	$\xrightarrow{76.9 (119.9)}$			SmA	$\xrightarrow{115.3 (2.6)}$	I
						$\xleftarrow{54.3 (74.2)}$		
	14	Cr	$\xrightarrow{66.8 (93.7)}$			SmA	$\xrightarrow{93.7 (2.2)}$	I
					$\xleftarrow{38.6 (84.6)}$			
	12	Cr	$\xrightarrow{56.3 (72.0)}$			SmA	$\xrightarrow{52.8 (1.3)}$	I
						$\xleftarrow{16.7 (48.2)}$		
	10	Cr	$\xrightarrow{37.9 (57.0)}$				$\xleftarrow{< 0.0}$	I
[C <sub>n</sub> PyOC <sub>n</sub> ][BF <sub>4</sub> ]	n = 18	Cr	$\xrightarrow{69.8 (67.0)}$			SmA	$\xrightarrow{127.9 (2.4)}$	I
						$\xleftarrow{57.0 (64.0)}$		
	16	Cr	$\xrightarrow{63.0 (62.3)}$			SmA	$\xrightarrow{113.5 (2.1)}$	I
						$\xleftarrow{43.4 (57.2)}$		
	14	Cr	$\xrightarrow{51.2 (63.9)}$			SmA	$\xrightarrow{98.2 (2.0)}$	I
					$\xleftarrow{23.2 (34.6)}$			
	12	Cr	$\xrightarrow{39.4 (47.4)}$			SmA	$\xrightarrow{77.3 (1.8)}$	I
					$\xleftarrow{5.8 (37.2)}$			
	10	Cr	$\xrightarrow{46.8 (66.1)}$				$\xleftarrow{< 0.0}$	I
[C <sub>n</sub> PyOH][Cl]	n = 18	Cr	$\xrightarrow{87.0 (82.9)}$			SmA	$\xrightarrow{157.1 (1.0)}$	I
						$\xleftarrow{47.2 (33.3)}$		
	16	Cr	$\xrightarrow{84.5 (76.9)}$			SmA	$\xrightarrow{114.9 (2.6)}$	I
					$\xleftarrow{43.9 (31.2)}$			
[HPyOC <sub>n</sub> ][Cl]	14	Cr	$\xrightarrow{79.2 (117.8)}$				$\xleftarrow{15.5 (35.2)}$	I
	12	Cr	$\xrightarrow{74.0 (104.2)}$				$\xleftarrow{< 0.0}$	I
	n = 18	Cr	$\xrightarrow{93.2 (15.1)}$	Cr*	$\xrightarrow{124.0 (60.0)}$	SmA	$\xrightarrow{142.6 (1.0)}$	I <sub>d</sub>
	16	Cr	$\xrightarrow{94.5 (14.4)}$	Cr*	$\xrightarrow{124.2 (49.0)}$	SmA	$\xrightarrow{142.0 (1.1)}$	I <sub>d</sub>
14	Cr	$\xrightarrow{95.1 (29.4)}$	Cr*	$\xrightarrow{122.4 (56.4)}$	SmA	$\xrightarrow{139.3 (2.1)}$	I <sub>d</sub>	
12	Cr	$\xrightarrow{92.4 (33.3)}$	Cr*	$\xrightarrow{121.8 (39.7)}$	SmA	$\xrightarrow{132.5 (1.5)}$	I <sub>d</sub>	

**Table 2** The *d*-spacings of pyridinium salts from powder X-ray diffraction. (RT = room temperature)

Compounds	<i>n</i>	<i>d</i> -Spacing/Å (T/°C)	
		Solid state	Meosphase
[C <sub><i>n</i></sub> PyOC <sub><i>n</i></sub> ][Br]	18	37.1 (RT)	37.1 (100)
	16	33.2 (RT)	33.8 (100)
	14	29.7 (RT)	29.9 (100)
	12	26.9 (RT)	27.1 (100)
	10	23.3 (RT)	22.8 (100)
[C <sub><i>n</i></sub> PyOC <sub><i>n</i></sub> ][PF <sub>6</sub> ]	18	26.2 (RT)	31.2 (100)
	16	23.9 (RT)	28.8 (100)
	14	21.3 (RT)	25.8 (85)
[C <sub><i>n</i></sub> PyOC <sub><i>n</i></sub> ][BF <sub>4</sub> ]	18	29.2 (RT)	32.2 (90)
	16	25.6 (RT)	29.7 (90)
	14	23.1 (RT)	26.9 (90)
	12	20.5 (RT)	24.3 (70)
[C <sub><i>n</i></sub> PyOH][Cl]	18	31.8 (RT)	34.1 (90)
	16	29.5 (RT)	31.7 (90)
[HPyOC <sub><i>n</i></sub> ][Cl]	18	30.9 (RT)	37.4 (130)
	16	28.3 (RT)	35.1 (130)
	14	25.7 (RT)	33.0 (130)
	12	23.5 (RT)	32.1 (130)

**Fig. 4** The PXR spectrum of [C<sub>16</sub>PyOC<sub>16</sub>][Br].**Scheme 4** Schematic drawing of [C<sub>16</sub>PyOC<sub>16</sub>][Br]; (a) at the crystal phase, (b) at the mesophase (100 °C).

142.6, 142.0, 139.3 and 132.5 °C accompanied by decompositions near the clearing points; nevertheless, the enthalpy changes are still observable. The melting and isotropic points are very insensitive to the chain lengths, suggesting that the hydrophobic interactions are the least significant factor in the thermal behavior of the [HPyOC<sub>*n*</sub>][Cl] series. The PXR experiments show that the compound of *n* = 16 has a layer distance of 28.3 Å at room temperature, consistent with an interdigitated bilayer

**Fig. 5** The texture of [C<sub>16</sub>PyOC<sub>16</sub>][PF<sub>6</sub>] at the mesophase (99 °C) upon heating.**Scheme 5** Schematic drawing of transitions of [C<sub>16</sub>PyOH][Cl]; (a) at the crystal phase, (b) at the mesophase (100 °C).

packing, similar to that of [C<sub>16</sub>PyOH][Cl]. Upon heated to 130 °C in the mesophase, an elongation of the layer distance to 35.1 Å is observed. For all the compounds of [HPyOC<sub>*n*</sub>][Cl], an increment of layer spacing of *ca.* 7 Å from the solid state to the mesophase is always found. This result suggests a structure of a non-interdigitated lamellar mesophase.

Thermal behaviors of these compounds are compared. Anions play an important role in the structure and mesophase behavior for the dialkylated pyridinium compounds. The PF<sub>6</sub><sup>-</sup> and BF<sub>4</sub><sup>-</sup> ions are unable to sustain ordered ionic motion for the chain length of *n* = 10; only at a chain length of *n* ≥ 12 do hydrophobic and ionic interactions come into play for the formation of the liquid crystals. This anion effect has been reported in other pyridinium salts.<sup>13f</sup> The ionic size also affects the crystal packing and mesophase structure. Thus for dialkyl substituted bromide compounds, a non-interdigitated monolayer structure is adopted in the crystal state and mesophase, whereas for the PF<sub>6</sub><sup>-</sup> and BF<sub>4</sub><sup>-</sup> salts, interdigitated structures are found in the crystalline state and partially interdigitated structures are adopted in the mesophase. Presumably, the larger anion allows the chain interdigitation to have efficient chain–chain hydrophobic interactions. Interestingly, while the two mono-alkylated C<sub>*n*</sub>PyO and PyOC<sub>*n*</sub> are non-mesomorphic, their protonated products do show liquid crystalline properties, an indication of the role of ionic interaction in the formation of the mesophase. Of these two

series of products,  $[C_n\text{PyOH}][\text{Cl}]$  exhibits a wider mesophase range than the  $[\text{HPyOC}_n][\text{Cl}]$  series, presumably the former have stronger cation–anion interactions. Although the latter series of compounds display a narrower mesophase range, all of them are mesomorphic. This is not the case for the former, only the compounds of  $n = 16$  and 18 are mesomorphic. These results suggest that the flexible chain has to be long enough to disrupt the strong ionic interactions to initial and maintain the mesophase. Similar *N*-protonated compounds  $[\text{HPyC}_{12}][X]$  ( $X = \text{Cl}$ , Br and I) are known,<sup>13a</sup> however, they are non-mesomorphic. Here, the oxygen atom in the alkoxy chain of  $[\text{HPyOC}_{12}][\text{Cl}]$  plays an important role in the formation of the mesophase. Presumably, the oxygen atom provides richer hydrogen bonding interactions to promote the formation of the mesophase.

### Aggregation in solution

The self-assembly properties of molecules in solution were studied employing the technique of diffusion-ordered spectroscopy (DOSY) NMR at various concentrations. The diffusion of chemical molecules in a solvent can be measured using the pulsed-field gradients. Depending on the size, shape, and concentration of the compounds in solution, the diffusion constants ( $D$ ) obtained by the Stokes–Einstein equation can be applied to get the relative average hydrodynamic radius ( $R_H$ ).<sup>20</sup>  $R_H$  is the radius of a hypothetical sphere that diffuses with the same speed as the particle under examination. In this text, two neutral compounds  $\text{PyOC}_{16}$  and  $\text{C}_{16}\text{PyO}$ , and three ionic compounds  $[\text{HPyOC}_{16}][\text{Cl}]$ ,  $[\text{C}_{16}\text{PyOH}][\text{Cl}]$  and  $[\text{C}_{16}\text{PyOC}_{16}][\text{Br}]$  were studied to measure the  $D$  and  $R_H$  values (Table 3). For the neutral compounds,  $\text{PyOC}_{16}$  and  $\text{C}_{16}\text{PyO}$ , the  $D$  values change only slightly upon varying its concentration from 12.5 to 100 mM. When HCl was added, these two pyridinium salts exhibit the concentration-dependent self-assembly phenomena in solution. For  $[\text{HPyOC}_{16}][\text{Cl}]$ , the diffusion coefficient of  $8.4 \times 10^{-10} \text{ m}^2 \text{ s}^{-1}$  ( $R_H = 4.7 \text{ \AA}$ ) at the concentration of 12.5 mM increases gradually to  $6.4 \times 10^{-10} \text{ m}^2 \text{ s}^{-1}$  ( $R_H = 6.2 \text{ \AA}$ ) at 100 mM. For the other protonated compound  $[\text{C}_{16}\text{PyOH}][\text{Cl}]$ , the diffusion coefficient increases from  $7.0 \times 10^{-10} \text{ m}^2 \text{ s}^{-1}$  ( $R_H = 5.7 \text{ \AA}$ ) at 12.5 mM to  $5.2 \times 10^{-10} \text{ m}^2 \text{ s}^{-1}$  ( $R_H = 7.6 \text{ \AA}$ ) at 50 mM. The diffusion rate of  $[\text{C}_{16}\text{PyOH}][\text{Cl}]$  at 100 mM is not measured, due to the solubility constrain. For the dialkylated ionic compound  $[\text{C}_{16}\text{PyOC}_{16}][\text{Br}]$ , the  $^1\text{H}$  chemical shift changes and diffusion coefficients are also concentration dependent (Fig. S1†). The  $R_H$  value is doubled (9.2  $\text{\AA}$ ) from 12.5 mM ( $R_H = 4.4 \text{ \AA}$ ) to 100 mM.

Although all these salts show concentration dependent  $D$  and  $R_H$  values, this behavior is more pronounced for the dialkylated salt than for the monoalkylated compounds, and suggests that the degree of aggregation is greater for the dialkylated salt than the monoalkylated salts. This could possibly be due to the additional hydrophobic interactions provided by the second alkyl chain in the dialkylated salt. A similar concentration-dependent behavior has been found for 1-(4-dodecyloxybenzyl)-3-methyl-1*H*-imidazolium bromide<sup>11e</sup> and 3,3'-hexadecyl-1,1'-(1,3-mesitylene)-bis(methylene)imidazolium iodide.<sup>21</sup>

### Stabilization of gold nanoparticles

Studies of gold nanoparticles (AuNPs) have been the subject of great research interest, due to their unique size- and shape-dependent properties, and have potential applications in catalysis, biology, and nanotechnology.<sup>22</sup> To prepare stable colloidal AuNPs in solution, stabilizers are usually required. Other than the commonly used thiols,<sup>23</sup> phosphines,<sup>24</sup> imidazolium salts,<sup>3e, 3g, 25</sup> and the *N*-monoalkylated pyridinium salt, 4-(dimethylamino)pyridine have also been used to stabilize AuNPs.<sup>26</sup> In this work, the dialkylated salt  $[\text{C}_{16}\text{PyOC}_{16}][\text{BF}_4]$  was examined for its ability to stabilize AuNPs.  $\text{HAuCl}_4$  mixed with pyridinium salts in  $\text{CH}_2\text{Cl}_2$  was stirred until the solution becomes clear. Then an aqueous  $\text{NaBH}_4$  solution was added to reduce the gold complex, after which the  $\text{CH}_2\text{Cl}_2$  layer turned ruby red indicating the formation of AuNPs. This colloidal gold solution is stable over months in air. This is in contrast to the previous observation that AuNPs stabilized by octadecylamine and triphenylphosphine could be stabilized for only a few days in chlorinated solvents.<sup>27</sup> This colloidal gold shows a strong surface plasmon band<sup>28</sup> at 524 nm in the UV-Vis spectrum (Fig. 6(a)). Under a transmission electron microscope (TEM), samples prepared by dipping the colloidal solution onto a copper grid reveals spherical AuNPs of *ca.* 8 nm assembled in a well ordered 2D array (Fig. 6(b)). The nature of  $[\text{C}_{16}\text{PyOC}_{16}][\text{BF}_4]$  on the surface of AuNPs was also studied by  $^1\text{H}$ -NMR spectroscopy. Signals between 0.5 and 2.0 ppm, assignable to alkyl chains are broad, and signals for the pyridinium ring essentially disappear (Fig. S2†), indicating that the pyridinium ring head is close to the surface of AuNP and the alkyl chains are stretched away from the AuNP (Fig. 6(c)). This argument is supported by the studies of FT-IR where the signals due to the pyridinium ring of AuNPs are barely observed, in contrast to those sharp bands observed for the free stabilizer (Fig. S3†). Moreover, the TEM image also shows that the

**Table 3** Diffusion coefficient values obtained for *N*- or *O*-substituted pyridine and pyridinium salt at different concentrations in  $\text{CDCl}_3$ .

Concentrations (mM)	Diffusion coefficient <sup>a</sup> (Hydrodynamic radius) <sup>b</sup>				
	$\text{PyOC}_{16}$	$\text{C}_{16}\text{PyO}$	$[\text{HPyOC}_{16}][\text{Cl}]$	$[\text{C}_{16}\text{PyOH}][\text{Cl}]$	$[\text{C}_{16}\text{PyOC}_{16}][\text{Br}]$
12.5	13.1(3.0)	9.7(4.1)	8.4(4.7)	7.0(5.7)	9.1(4.4)
25.0	10.2(3.9)	8.8(4.5)	7.9(5.0)	6.6(6.0)	6.6(6.1)
50.0	10.4(3.8)	8.9(4.5)	6.9(5.8)	5.2(7.6)	5.8(6.9)
100.0	10.4(3.8)	8.6(4.6)	6.4(6.2)		4.3(9.2)

<sup>a</sup> In units of  $10^{-10} \text{ m}^2 \text{ s}^{-1}$ . Measured at 25 °C in  $\text{CDCl}_3$  (viscosity = 0.55  $\text{kg s}^{-1} \text{ m}$ ). Data were measured using the double-STE pulse sequence using a diffusion time of 50 ms and bipolar gradients with duration of 1 ms. The sample was not spun. Data were acquired and processed using the automation programs included in the TOPSPIN software package. 16 spectra were acquired using a linear gradient ramp from 2 to 95% using sine-shaped gradients. <sup>b</sup> In units of  $10^{-10} \text{ m}$ . The values were obtained after applying the Stokes–Einstein equation.

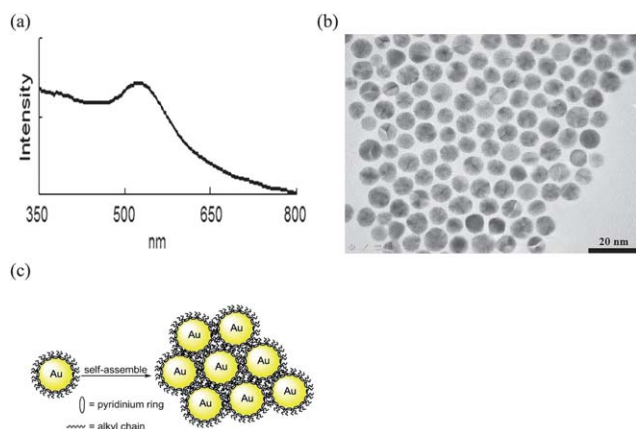


**Fig. 6** (a) The UV-Vis spectrum of AuNPs and the absorption is 524 nm. (b) The TEM image for AuNPs stabilized by  $[C_{16}PyOC_{16}][BF_4]$  in  $CH_2Cl_2$ . (c) The diagram for pyridinium salts protect the AuNPs.

distance between the particles is *ca.* 2 nm, which is consistent with the spacing of a bilayered packing of U-shaped  $[C_{16}PyOC_{16}][BF_4]$ .

## Conclusion

*N*-Alkylpyridones  $C_nPyO$  and *O*-alkoxy pyridines  $PyOC_n$  are prepared in good yields *via* controlled alkylation. Both the neutral compounds of  $C_nPyO$  and  $PyOC_n$  are non-mesomorphic. However, upon further reaction with alkyl bromide produce dialkylated pyridinium salts possessing LC properties. Protonating the two neutral series of compounds also induce an SmA LC phase; which has the potential to serve as proton transfer materials with directional order. Dialkylated pyridinium salts have a similar mesophase temperature range comparable to those of other reported pyridinium salts with a single core. The effect of an anion on the mesophase range of *N*-alkyl-4-alkoxy pyridinium salts is  $Br^- > BF_4^- > PF_6^-$ . The larger sized anions ( $PF_6^-$  and  $BF_4^-$ ) favor the assembly *via* interdigitated alkyl chains in the solid, and partial interdigitation in the mesophase. While the pyridinium salts of  $[HPyOC_{16}][Cl]$ ,  $[C_{16}PyOH][Cl]$  and  $[C_{16}PyOC_{16}][Br]$  display concentration-dependent aggregation in  $CDCl_3$ , the neutral compounds of  $PyOC_{16}$  and  $C_{16}PyO$  are not. Finally,  $[C_{16}PyOC_{16}][BF_4]$  is a good stabilizer for spherical AuNPs (*ca.* 8 nm) in  $CH_2Cl_2$  for months. Here, we provide an alternative facile route for the synthesis of stable AuNPs without adding other phase transfer agents such as tetraoctylammonium bromide (TOAB).

## Experimental section

All the solvents and reagents were purchased from Aldrich, Acros, J. T. Baker and used as received.  $^1H$ -NMR (300 & 400 MHz) spectra were recorded on an Avance DPX<sub>300</sub> BRUKER, Avance<sup>II</sup> 400 BRUKER and the chemical shifts ( $\delta$ ) were given in ppm and referenced to residual solvent signals. Elemental analyses were performed in the Taiwan Instrument Center. In this content, the phase transitions and thermodynamic data were determined by differential scanning calorimetry (Mettler Toledo DSC822 equipped with cryostatic cooling,

3–5 mg samples,  $10\text{ }^\circ\text{C min}^{-1}$  heating and cooling rates and calibrated with indium and tin standards). Optical characterization of the pyridinium salts were performed by a Zeiss Axio-plan 2 polarizing microscope equipped with a Mettler Toledo FP82 hot stage and Mettler Toledo FP90 central processor. The powder X-ray diffraction data were determined from the Wiggler-A beamline of the National Synchrotron Radiation Research Center (NSRRC). Diffraction patterns were recorded in  $\theta/2\theta$  geometry with step scans normally  $0.02$  degree in  $2\theta = 1\text{--}25$  degree  $\text{step}^{-1} \text{ s}^{-1}$  and a gas flow heater was used to control the temperature. The powder samples were charged in Lindemann capillary tubes (80 mm long and 0.01 mm thick) from Charles Supper Co. with an inner diameter of 0.10 or 0.15 mm. Single crystal X-ray diffraction data were collected on a Bruker SMART diffractometer equipped with a CCD array detector with graphite monochromatized Mo- $K\alpha$  radiation ( $\lambda = 0.71073\text{ \AA}$ ) in  $\varphi$  and  $\omega$  scan modes. FT-IR spectra were measured with a Mattson Galaxy Series FT-IR 3000 spectrophotometer. The UV-Vis spectra were obtained on a PerkinElmer Lambda 750 spectrophotometer. The images of nanoparticles were acquired by an Analytical Transmission Electron Microscope (JEOL JEM-3010). All diffusion NMR experiments were acquired at 298 K on a BRUKER 600 UltraShield<sup>TM</sup> equipped with a 5 mm BBO inverseprobe. Diffusion experiments were performed with a diffusion time of 50 ms and a longitudinal Eddy-current delay (LED) of 5 ms. Hydrodynamic radii were obtained through the Stokes–Einstein equation ( $D = kT/6\pi\eta R_H$ ),  $D$  is the diffusion coefficient ( $\text{m}^2 \text{ s}^{-1}$ ),  $k$  is the Boltzmann constant ( $\text{m}^2 \text{ kg s}^{-2} \text{ K}^{-1}$ ),  $T$  is the absolute temperature (K),  $\eta$  is the viscosity of solvent ( $\text{kg s}^{-1} \text{ m}^{-1}$ ) and  $R_H$  is the hydrodynamic radius (m).

## General method for the synthesis of *N*-alkyl-4-pyridone monohydrate

To a mixture of 4-hydroxypyridine (5.00 g, 52.57 mmol) and tetrabutylammonium bromide (TBAB) (1.69 g, 5.24 mmol) in 50 mL THF was added with an aqueous NaOH solution (2N, 25 mL). This resultant solution was stirred until the muddy solution became clear. 1-Bromooctadecane (14.01 g, 42.05 mmol) was then added to this solution with refluxing for 24 h at  $75\text{ }^\circ\text{C}$ . After cooling, the THF solvent was removed by a rotary evaporator, and the crude product was extracted by  $CH_2Cl_2$  and water (1 : 0.8). The organic layer was collected and the  $CH_2Cl_2$  was removed by a rotary evaporator. The crude product was treated with ether, and then filtered by gravitation the filtrate collected, because  $[C_{18}PyO]\cdot H_2O$  was dissolved in ether. This step was repeated several times. The ether solvent was removed and a white product was obtained *N*-octadecyl-4-pyridone with a yield of about 80%.  $^1H$ -NMR (300 MHz,  $CDCl_3$ ):  $\delta = 0.87$  (t,  $^3J = 7$  Hz, 3H,  $CH_3$ ), 1.24–1.44 (m, 30H,  $CH_2$ ), 1.77 (t,  $^3J = 7$  Hz, 2H,  $CH_2$ ), 3.81 (t,  $^3J = 7$  Hz, 2H,  $CH_2$ ), 6.46 (d,  $^3J = 7$  Hz, 2H, aromatic CH), 7.35 (d,  $^3J = 7$  Hz, 2H, aromatic CH). Anal. calcd. for  $C_{23}H_{43}NO_2$ : C 75.56; H 11.85; N 3.83. Found: C 75.43; H 11.75; N 3.74%.

***N*-Hexadecyl-4-pyridone.** Typical data for  $[C_{16}PyO]\cdot H_2O$ : white solid, yield 76%.  $^1H$ -NMR (300 MHz,  $CDCl_3$ ):  $\delta = 0.84$  (t,  $^3J = 7$  Hz, 3H,  $CH_3$ ), 1.24–1.29 (m, 26H,  $CH_2$ ), 1.76 (t,  $^3J = 7$

Hz, 2H, CH<sub>2</sub>), 3.79 (t, <sup>3</sup>J = 7 Hz, 2H, CH<sub>2</sub>), 6.45 (d, <sup>3</sup>J = 7 Hz, 2H, aromatic CH), 7.32 (d, <sup>3</sup>J = 7 Hz, 2H, aromatic CH). Anal. calcd. for C<sub>21</sub>H<sub>39</sub>NO<sub>2</sub>: C 74.72; H 11.65; N 4.15. Found: C 75.09; H 11.70; N 4.13%.

**N-Tetradecyl-4-pyridone.** Typical data for [C<sub>14</sub>PyO]·H<sub>2</sub>O: white solid, yield 75%. <sup>1</sup>H-NMR (300 MHz, CDCl<sub>3</sub>): δ = 0.87 (t, <sup>3</sup>J = 7 Hz, 3H, CH<sub>3</sub>), 1.25–1.30 (m, 22H, CH<sub>2</sub>), 1.76 (t, <sup>3</sup>J = 7 Hz, 2H, CH<sub>2</sub>), 3.75 (t, <sup>3</sup>J = 7 Hz, 2H, CH<sub>2</sub>), 6.39 (d, <sup>3</sup>J = 7 Hz, 2H, aromatic CH), 7.28 (d, <sup>3</sup>J = 7 Hz, 2H, aromatic CH). Anal. calcd. for C<sub>19</sub>H<sub>35</sub>NO<sub>2</sub>: C 73.74; H 11.40; N 4.53. Found: C 73.56; H 11.50; N 4.45%.

**N-Dodecyl-4-pyridone.** Typical data for [C<sub>12</sub>PyO]·H<sub>2</sub>O: white solid, yield 76%. <sup>1</sup>H-NMR (300 MHz, CDCl<sub>3</sub>): δ = 0.87 (t, <sup>3</sup>J = 7 Hz, 3H, CH<sub>3</sub>), 1.24–1.29 (m, 18H, CH<sub>2</sub>), 1.75 (t, <sup>3</sup>J = 7 Hz, 2H, CH<sub>2</sub>), 3.75 (t, <sup>3</sup>J = 7 Hz, 2H, CH<sub>2</sub>), 6.38 (d, <sup>3</sup>J = 7 Hz, 2H, aromatic CH), 7.29 (d, <sup>3</sup>J = 7 Hz, 2H, aromatic CH). Anal. calcd. for C<sub>17</sub>H<sub>31</sub>NO<sub>2</sub>: C 72.55; H 11.10; N 4.98. Found: C 72.91; H 11.27; N 5.00%.

#### General method for the synthesis of 4-alkoxyppyridinium hydrochloride

A mixture of [PyOC<sub>18</sub>] (0.20 g, 0.58 mmol) was dissolved in 25 mL of methanol and added 1 mL of concentration of hydrochloric acid (HCl) with stirring at room temperature for 40 h. Then the methanol solvent was removed by a rotary evaporator. The residual HCl was removed under vacuum at 50 °C and then we could get a white product 4-octadecyloxyppyridinium hydrochloride with a yield of about 98%. Typical data for [HPyOC<sub>18</sub>][Cl]·0.5H<sub>2</sub>O: <sup>1</sup>H-NMR (400 MHz, CDCl<sub>3</sub>): δ = 0.88 (t, <sup>3</sup>J = 7 Hz, 3H, CH<sub>3</sub>), 1.25–1.36 (m, 28H, CH<sub>2</sub>), 1.44–1.50 (m, 2H, CH<sub>2</sub>), 1.86–1.91 (m, 2H, CH<sub>2</sub>), 4.24 (t, <sup>3</sup>J = 6 Hz, 2H, CH<sub>2</sub>), 7.22 (d, <sup>3</sup>J = 6 Hz, 2H, aromatic), 8.55 (d, <sup>3</sup>J = 6 Hz, 2H, aromatic). Anal. calcd. for C<sub>23</sub>H<sub>42</sub>NOCl·0.5H<sub>2</sub>O: C 70.28; H 11.03; N 3.56. Found: C 70.16; H 10.90; N 3.39%.

**4-Hexadecyloxyppyridinium hydrochloride.** Typical data for [HPyOC<sub>16</sub>][Cl]·0.5H<sub>2</sub>O: white solid, yield 91%. <sup>1</sup>H-NMR (400 MHz, CDCl<sub>3</sub>): δ = 0.87 (t, <sup>3</sup>J = 7 Hz, 3H, CH<sub>3</sub>), 1.25–1.35 (m, 24H, CH<sub>2</sub>), 1.44–1.50 (m, 2H, CH<sub>2</sub>), 1.86–1.91 (m, 2H, CH<sub>2</sub>), 4.24 (t, <sup>3</sup>J = 7 Hz, 2H, CH<sub>2</sub>), 7.22 (d, <sup>3</sup>J = 7 Hz, 2H, aromatic), 8.56 (d, <sup>3</sup>J = 6 Hz, 2H, aromatic). Anal. calcd. for C<sub>21</sub>H<sub>38</sub>NOCl·0.5H<sub>2</sub>O: C 69.10; H 10.77; N 3.84. Found: C 68.81; H 10.74; N 3.80%.

**4-Tetradecyloxyppyridinium hydrochloride.** Typical data for [HPyOC<sub>14</sub>][Cl]·0.5H<sub>2</sub>O: white solid, yield 93%. <sup>1</sup>H-NMR (400 MHz, CDCl<sub>3</sub>): δ = 0.87 (t, <sup>3</sup>J = 7 Hz, 3H, CH<sub>3</sub>), 1.26–1.36 (m, 20H, CH<sub>2</sub>), 1.46–1.51 (m, 2H, CH<sub>2</sub>), 1.87–1.91 (m, 2H, CH<sub>2</sub>), 4.24 (t, <sup>3</sup>J = 6 Hz, 2H, CH<sub>2</sub>), 7.23 (d, <sup>3</sup>J = 6 Hz, 2H, aromatic), 8.57 (d, <sup>3</sup>J = 7 Hz, 2H, aromatic). Anal. calcd. for C<sub>19</sub>H<sub>34</sub>NOCl·0.5H<sub>2</sub>O: C 67.73; H 10.47; N 4.16. Found: C 67.62; H 10.54; N 4.03%.

**4-Dodecyloxyppyridinium hydrochloride.** Typical data for [HPyOC<sub>12</sub>][Cl]·H<sub>2</sub>O: white solid, yield 91%. <sup>1</sup>H-NMR (400 MHz, CDCl<sub>3</sub>): δ = 0.89 (t, <sup>3</sup>J = 7 Hz, 3H, CH<sub>3</sub>), 1.26–1.38

(m, 16H, CH<sub>2</sub>), 1.44–1.51 (m, 2H, CH<sub>2</sub>), 1.86–1.93 (m, 2H, CH<sub>2</sub>), 4.24 (t, <sup>3</sup>J = 6 Hz, 2H, CH<sub>2</sub>), 7.23 (d, <sup>3</sup>J = 7 Hz, 2H, aromatic), 8.57 (d, <sup>3</sup>J = 7 Hz, 2H, aromatic). Anal. calcd. for C<sub>17</sub>H<sub>32</sub>NO<sub>2</sub>Cl: C 64.23; H 10.15; N 4.41. Found: C 64.79; H 10.16; N 4.39%.

#### General method for the synthesis of N-alkyl-4-alkoxyppyridinium bromide monohydrate

A mixture of [C<sub>18</sub>PyO]·H<sub>2</sub>O (1.00 g, 2.74 mmol) and 1-bromooctadecane (1.08 g, 3.26 mmol) was treated with stirring at 85 °C for 24 h without adding any solvent. After cooling, the solid was obtained and hexane added to remove the remaining 1-bromooctadecane. The crude product was obtained by filtration. Recrystallization from CH<sub>2</sub>Cl<sub>2</sub> and ether gave the white solid of N-octadecyl-4-octadecyloxyppyridinium bromide with a yield of about 83%. Typical data for [C<sub>18</sub>PyOC<sub>18</sub>][Br]·H<sub>2</sub>O: <sup>1</sup>H-NMR (400 MHz, CDCl<sub>3</sub>): δ = 0.85 (t, <sup>3</sup>J = 7 Hz, 6H, CH<sub>3</sub>), 1.21–1.44 (m, 60H, CH<sub>2</sub>), 1.80–1.94 (m, 4H, CH<sub>2</sub>), 4.27 (t, <sup>3</sup>J = 6 Hz, 2H, CH<sub>2</sub>), 4.69 (t, <sup>3</sup>J = 7 Hz, 2H, CH<sub>2</sub>), 7.43 (d, <sup>3</sup>J = 7 Hz, 2H, aromatic CH), 9.13 (d, <sup>3</sup>J = 7 Hz, 2H, aromatic CH). Anal. calcd. for C<sub>41</sub>H<sub>80</sub>NO<sub>2</sub>Br: C 70.45; H 11.54; N 2.00. Found: C 70.38; H 11.60; N 1.98%.

**N-Hexadecyl-4-hexadecyloxyppyridinium bromide.** Typical data for [C<sub>16</sub>PyOC<sub>16</sub>][Br]·H<sub>2</sub>O: white solid, yield 85%. <sup>1</sup>H-NMR (400 MHz, CDCl<sub>3</sub>): δ = 0.87 (t, <sup>3</sup>J = 7 Hz, 6H, CH<sub>3</sub>), 1.22–1.46 (m, 52H, CH<sub>2</sub>), 1.84–1.96 (m, 4H, CH<sub>2</sub>), 4.28 (t, <sup>3</sup>J = 6 Hz, 2H, CH<sub>2</sub>), 4.69 (t, <sup>3</sup>J = 7 Hz, 2H, CH<sub>2</sub>), 7.43 (d, <sup>3</sup>J = 7 Hz, 2H, aromatic CH), 9.07 (d, <sup>3</sup>J = 7 Hz, 2H, aromatic CH). Anal. calcd. for C<sub>37</sub>H<sub>72</sub>NO<sub>2</sub>Br: C 69.13; H 11.29; N 2.18. Found: C 68.93; H 11.30; N 2.12%.

**N-Tetradecyl-4-tetradecyloxyppyridinium bromide.** Typical data for [C<sub>14</sub>PyOC<sub>14</sub>][Br]·H<sub>2</sub>O: white solid, yield 83%. <sup>1</sup>H-NMR (400 MHz, CDCl<sub>3</sub>): δ = 0.86 (t, <sup>3</sup>J = 7 Hz, 6H, CH<sub>3</sub>), 1.22–1.45 (m, 44H, CH<sub>2</sub>), 1.81–1.93 (m, 4H, CH<sub>2</sub>), 4.28 (t, <sup>3</sup>J = 6 Hz, 2H, CH<sub>2</sub>), 4.68 (t, <sup>3</sup>J = 7 Hz, 2H, CH<sub>2</sub>), 7.44 (d, <sup>3</sup>J = 7 Hz, 2H, aromatic CH), 9.08 (d, <sup>3</sup>J = 7 Hz, 2H, aromatic CH). Anal. calcd. for C<sub>33</sub>H<sub>64</sub>NO<sub>2</sub>Br: C 67.55; H 10.99; N 2.39. Found: C 67.54; H 11.06; N 2.34%.

**N-Dodecyl-4-dodecyloxyppyridinium bromide.** Typical data for [C<sub>12</sub>PyOC<sub>12</sub>][Br]·H<sub>2</sub>O: white solid, yield 84%. <sup>1</sup>H-NMR (400 MHz, CDCl<sub>3</sub>): δ = 0.86 (t, <sup>3</sup>J = 7 Hz, 6H, CH<sub>3</sub>), 1.25–1.47 (m, 36H, CH<sub>2</sub>), 1.87 (m, 4H, CH<sub>2</sub>), 4.28 (t, <sup>3</sup>J = 6 Hz, 2H, CH<sub>2</sub>), 4.68 (t, <sup>3</sup>J = 7 Hz, 2H, CH<sub>2</sub>), 7.44 (d, <sup>3</sup>J = 7 Hz, 2H, aromatic CH), 9.10 (d, <sup>3</sup>J = 7 Hz, 2H, aromatic CH). Anal. calcd. for C<sub>29</sub>H<sub>56</sub>NO<sub>2</sub>Br: C 65.64; H 10.64; N 2.64. Found: C 65.41; H 10.66; N 2.59%.

**N-Decyl-4-decyloxyppyridinium bromide.** Typical data for [C<sub>10</sub>PyOC<sub>10</sub>][Br]·H<sub>2</sub>O: white solid, yield 80%. <sup>1</sup>H-NMR (400 MHz, CDCl<sub>3</sub>): δ = 0.87 (t, <sup>3</sup>J = 7 Hz, 6H, CH<sub>3</sub>), 1.25–1.40 (m, 28H, CH<sub>2</sub>), 1.87 (m, 4H, CH<sub>2</sub>), 4.26 (t, <sup>3</sup>J = 6 Hz, 2H, CH<sub>2</sub>), 4.67 (t, <sup>3</sup>J = 7 Hz, 2H, CH<sub>2</sub>), 7.45 (d, <sup>3</sup>J = 7 Hz, 2H, aromatic CH), 9.12 (d, <sup>3</sup>J = 7 Hz, 2H, aromatic CH). Anal. calcd. for C<sub>25</sub>H<sub>48</sub>NO<sub>2</sub>Br: C 63.27; H 10.19; N 2.95. Found: C 63.47; H 10.30; N 2.71%.

### General method for the synthesis of *N*-alkyl-4-alkoxyppyridinium hexafluorophosphate

A mixture of  $[C_{18}PyOC_{18}][Br] \cdot H_2O$  (0.20 g, 0.30 mmol) was dissolved in 5 mL of 95% ethanol and ammonium hexafluorophosphate ( $NH_4PF_6$ ) (0.07 g, 0.45 mmol) was also dissolved in 5 mL of 95% ethanol with stirring at room temperature for 2 h. When the two solutions were mixed, the white precipitates appeared at once and the solid was obtained by filtration, and then the crude products were eluted by adding ethanol and water. Recrystallization from  $CH_2Cl_2$  and hexane gave the white solid of *N*-octadecyl-4-octadecyloxyppyridinium hexafluorophosphate with a yield of about 91%. Typical data for  $[C_{18}PyOC_{18}][PF_6]$ :  $^1H$ -NMR (300 MHz,  $CDCl_3$ ):  $\delta = 0.88$  (t,  $^3J = 7$  Hz, 6H,  $CH_3$ ), 1.25–1.45 (m, 60H,  $CH_2$ ), 1.86 (m, 4H,  $CH_2$ ), 4.26 (t,  $^3J = 6$  Hz, 2H,  $CH_2$ ), 4.37 (t,  $^3J = 8$  Hz, 2H,  $CH_2$ ), 7.37 (d,  $^3J = 7$  Hz, 2H, aromatic CH), 8.41 (d,  $^3J = 7$  Hz, 2H, aromatic CH). Anal. calcd. for  $C_{41}H_{78}NOPF_6$ : C 66.01; H 10.54; N 1.88. Found: C 65.47; H 10.49; N 1.91%.

#### *N*-Hexadecyl-4-hexadecyloxyppyridinium hexafluorophosphate.

Typical data for  $[C_{16}PyOC_{16}][PF_6]$ : white solid, yield 86%.  $^1H$ -NMR (300 MHz,  $CDCl_3$ ):  $\delta = 0.88$  (t,  $^3J = 7$  Hz, 6H,  $CH_3$ ), 1.25–1.46 (m, 52H,  $CH_2$ ), 1.84 (m, 4H,  $CH_2$ ), 4.26 (t,  $^3J = 6$  Hz, 2H,  $CH_2$ ), 4.37 (t,  $^3J = 8$  Hz, 2H,  $CH_2$ ), 7.32 (d,  $^3J = 7$  Hz, 2H, aromatic CH), 8.41 (d,  $^3J = 7$  Hz, 2H, aromatic CH). Anal. calcd. for  $C_{37}H_{70}NOPF_6$ : C 64.41; H 10.23; N 2.03. Found: C 64.06; H 10.23; N 2.07%.

#### *N*-Tetradecyl-4-tetradecyloxyppyridinium hexafluorophosphate.

Typical data for  $[C_{14}PyOC_{14}][PF_6]$ : white solid, yield 86%.  $^1H$ -NMR (300 MHz,  $CDCl_3$ ):  $\delta = 0.88$  (t,  $^3J = 7$  Hz, 6H,  $CH_3$ ), 1.24–1.45 (m, 44H,  $CH_2$ ), 1.84 (m, 4H,  $CH_2$ ), 4.26 (t,  $^3J = 6$  Hz, 2H,  $CH_2$ ), 4.37 (t,  $^3J = 7$  Hz, 2H,  $CH_2$ ), 7.32 (d,  $^3J = 7$  Hz, 2H, aromatic CH), 8.40 (d,  $^3J = 7$  Hz, 2H, aromatic CH). Anal. calcd. for  $C_{33}H_{62}NOPF_6$ : C 62.54; H 9.86; N 2.21. Found: C 62.01; H 9.87; N 2.23%.

#### *N*-Dodecyl-4-dodecyloxyppyridinium hexafluorophosphate.

Typical data for  $[C_{12}PyOC_{12}][PF_6]$ : white solid, yield 89%.  $^1H$ -NMR (300 MHz,  $CDCl_3$ ):  $\delta = 0.87$  (t,  $^3J = 7$  Hz, 6H,  $CH_3$ ), 1.24–1.45 (m, 36H,  $CH_2$ ), 1.86 (m, 4H,  $CH_2$ ), 4.26 (t,  $^3J = 6$  Hz, 2H,  $CH_2$ ), 4.37 (t,  $^3J = 7$  Hz, 2H,  $CH_2$ ), 7.32 (d,  $^3J = 7$  Hz, 2H, aromatic CH), 8.41 (d,  $^3J = 7$  Hz, 2H, aromatic CH). Anal. calcd. for  $C_{29}H_{54}NOPF_6$ : C 60.29; H 9.42; N 2.42. Found: C 60.41; H 9.31; N 2.36%.

***N*-Decyl-4-decyloxyppyridinium hexafluorophosphate.** Typical data for  $[C_{10}PyOC_{10}][PF_6]$ : white solid, yield 61%.  $^1H$ -NMR (300 MHz,  $CDCl_3$ ):  $\delta = 0.87$  (t,  $^3J = 7$  Hz, 6H,  $CH_3$ ), 1.25–1.45 (m, 28H,  $CH_2$ ), 1.88 (m, 4H,  $CH_2$ ), 4.25 (t,  $^3J = 6$  Hz, 2H,  $CH_2$ ), 4.36 (t,  $^3J = 7$  Hz, 2H,  $CH_2$ ), 7.32 (d,  $^3J = 7$  Hz, 2H, aromatic CH), 8.41 (d,  $^3J = 7$  Hz, 2H, aromatic CH). Anal. calcd. for  $C_{25}H_{46}NOPF_6$ : C 57.57; H 8.89; N 2.69. Found: C 57.22; H 8.91; N 2.69%.

### General method for the synthesis of *N*-alkyl-4-alkoxyppyridinium tetrafluoroborate

A mixture of  $[C_{18}PyOC_{18}][Br] \cdot H_2O$  (0.10 g, 0.15 mmol) was dissolved in 130 mL of 83% ethanol and ammonium

tetrafluoroborate ( $NH_4BF_4$ ) (0.04 g, 0.35 mmol) was dissolved in 20 mL of 83% ethanol with stirring at room temperature for 0.5 h. When the two solutions were mixed, the white precipitates appeared at once and the solid was obtained by filtration, and then the crude products were eluted by adding 83% ethanol and water. Recrystallization from  $CH_2Cl_2$  and hexane gave the white solid of *N*-octadecyl-4-octadecyloxyppyridinium tetrafluoroborate with a yield of about 85%. Typical data for  $[C_{18}PyOC_{18}][BF_4] \cdot 0.5H_2O$ :  $^1H$ -NMR (300 MHz,  $CDCl_3$ ):  $\delta = 0.88$  (t,  $^3J = 7$  Hz, 6H,  $CH_3$ ), 1.26–1.45 (m, 60H,  $CH_2$ ), 1.86 (m, 4H,  $CH_2$ ), 4.27 (t,  $^3J = 6$  Hz, 2H,  $CH_2$ ), 4.42 (t,  $^3J = 8$  Hz, 2H,  $CH_2$ ), 7.35 (d,  $^3J = 7$  Hz, 2H, aromatic CH), 8.52 (d,  $^3J = 7$  Hz, 2H, aromatic CH). Anal. calcd. for  $C_{41}H_{78}NOBF_4 \cdot 0.5H_2O$ : C 70.66; H 11.43; N 2.01. Found: C 70.84; H 11.29; N 2.10%.

#### *N*-Hexadecyl-4-hexadecyloxyppyridinium tetrafluoroborate.

Typical data for  $[C_{16}PyOC_{16}][BF_4]$ : white solid, yield 77%.  $^1H$ -NMR (300 MHz,  $CDCl_3$ ):  $\delta = 0.87$  (t,  $^3J = 7$  Hz, 6H,  $CH_3$ ), 1.25–1.45 (m, 52H,  $CH_2$ ), 1.85 (m, 4H,  $CH_2$ ), 4.25 (t,  $^3J = 6$  Hz, 2H,  $CH_2$ ), 4.36 (t,  $^3J = 8$  Hz, 2H,  $CH_2$ ), 7.31 (d,  $^3J = 7$  Hz, 2H, aromatic CH), 8.42 (d,  $^3J = 7$  Hz, 2H, aromatic CH). Anal. calcd. for  $C_{37}H_{70}NOBF_4$ : C 70.43; H 11.17; N 2.22. Found: C 69.94; H 11.13; N 2.25%.

#### *N*-Tetradecyl-4-tetradecyloxyppyridinium tetrafluoroborate.

Typical data for  $[C_{14}PyOC_{14}][BF_4]$ : white solid, yield 89%.  $^1H$ -NMR (300 MHz,  $CDCl_3$ ):  $\delta = 0.88$  (t,  $^3J = 7$  Hz, 6H,  $CH_3$ ), 1.24–1.45 (m, 44H,  $CH_2$ ), 1.83 (m, 4H,  $CH_2$ ), 4.27 (t,  $^3J = 6$  Hz, 2H,  $CH_2$ ), 4.43 (t,  $^3J = 8$  Hz, 2H,  $CH_2$ ), 7.36 (d,  $^3J = 7$  Hz, 2H, aromatic CH), 8.53 (d,  $^3J = 7$  Hz, 2H, aromatic CH). Anal. calcd. for  $C_{33}H_{62}NOBF_4$ : C 68.85; H 10.86; N 2.43. Found: C 68.84; H 10.96; N 2.48%.

***N*-Dodecyl-4-dodecyloxyppyridinium tetrafluoroborate.** Typical data for  $[C_{12}PyOC_{12}][BF_4]$ : white solid, yield 74%.  $^1H$ -NMR (300 MHz,  $CDCl_3$ ):  $\delta = 0.87$  (t,  $^3J = 7$  Hz, 6H,  $CH_3$ ), 1.23–1.45 (m, 36H,  $CH_2$ ), 1.83 (m, 4H,  $CH_2$ ), 4.26 (t,  $^3J = 6$  Hz, 2H,  $CH_2$ ), 4.41 (t,  $^3J = 7$  Hz, 2H,  $CH_2$ ), 7.35 (d,  $^3J = 7$  Hz, 2H, aromatic CH), 8.54 (d,  $^3J = 7$  Hz, 2H, aromatic CH). Anal. calcd. for  $C_{29}H_{54}NOBF_4$ : C 67.04; H 10.48; N 2.70. Found: C 66.71; H 10.42; N 2.34%.

***N*-Decyl-4-decyloxyppyridinium tetrafluoroborate.** Typical data for  $[C_{10}PyOC_{10}][BF_4]$ : white solid, yield 62%.  $^1H$ -NMR (300 MHz,  $CDCl_3$ ):  $\delta = 0.86$  (t,  $^3J = 7$  Hz, 6H,  $CH_3$ ), 1.23–1.45 (m, 28H,  $CH_2$ ), 1.88 (m, 4H,  $CH_2$ ), 4.25 (t,  $^3J = 6$  Hz, 2H,  $CH_2$ ), 4.36 (t,  $^3J = 7$  Hz, 2H,  $CH_2$ ), 7.31 (d,  $^3J = 7$  Hz, 2H, aromatic CH), 8.42 (d,  $^3J = 7$  Hz, 2H, aromatic CH). Anal. calcd. for  $C_{25}H_{46}NOBF_4$ : C 64.79; H 10.00; N 3.02. Found: C 64.75; H 9.96; N 2.70%.

### Formation of gold nanoparticles

The gold mixture was prepared from  $HAuCl_4$  (0.01 g, 0.03 mmol),  $[C_{16}PyOC_{16}][BF_4]$  (0.19 g, 0.30 mmol), and  $CH_2Cl_2$  (10 mL). After 1 h, when the solution became clear, an aqueous solution of  $NaBH_4$  was added ( $1.5 \times 10^{-3}$  M, 10 mL) with violent shaking. The colorless  $CH_2Cl_2$  solution changed to ruby red and the metallic nanoparticles were formed. The  $CH_2Cl_2$  layer was selected and the

solvent was removed, then the ethanol was added and was centrifuged at 9000 rpm for 10 min. Finally, the solvent was removed and the purple gold nanoparticle were obtained.

## Acknowledgements

We thank the National Science Council of Taiwan (Grant no. NSC 97-2113-M-259-009-MY3) for the financial support of this work.

## References

- 1 K. Binnemans, *Chem. Rev.*, 2005, **105**, 4148.
- 2 (a) T. Welton, *Chem. Rev.*, 1999, **99**, 2071; (b) P. Wasserscheid and W. Keim, *Angew. Chem., Int. Ed.*, 2000, **39**, 3772; (c) J. Dupont, R. F. De Souza and P. A. Z. Suarez, *Chem. Rev.*, 2002, **102**, 3667.
- 3 (a) J. Dupont, G. S. Fonseca, A. P. Umpierre, P. F. P. Fichtner and S. R. Teixeira, *J. Am. Chem. Soc.*, 2002, **124**, 4228; (b) J. Huang, T. Jiang, B. Han, H. Gao, Y. Chang, G. Zhao and W. Wu, *Chem. Commun.*, 2003, 1654; (c) C. W. Scheeren, G. Machado, J. Dupont, P. F. P. Fichtner and S. R. Teixeira, *Inorg. Chem.*, 2003, **42**, 4738; (d) A. Taubert, *Angew. Chem., Int. Ed.*, 2004, **43**, 5380; (e) H. Itoh, K. Naka and Y. Chujo, *J. Am. Chem. Soc.*, 2004, **126**, 3026; (f) A. Taubert, I. Arbell, A. Mecke and P. Graf, *Gold Bull.*, 2006, **39**, 205; (g) N. C. King, R. A. Blackley, W. Zhou and D. W. Bruce, *Chem. Commun.*, 2006, 3411; (h) W. Dobbs, M. J-Suisse, L. Douce and R. Welter, *Angew. Chem., Int. Ed.*, 2006, **45**, 4179; (i) D. Mumalo-Djokic, W. B. Stern and A. Taubert, *Cryst. Growth Des.*, 2008, **8**, 330.
- 4 D. J. Abdallah and R. G. Weiss, *Chem. Mater.*, 2000, **12**, 406.
- 5 (a) T. Kato, *Science*, 2002, **295**, 2414; (b) M. Yoshio, T. Mukai, H. Ohno and T. Kato, *J. Am. Chem. Soc.*, 2004, **126**, 994.
- 6 D. Demus, J. Goodby, G. W. Gray, H. W. Spiess and V. Vill, *Handbook of Liquid Crystals, Amphiphilic Liquid Crystals*, Wiley-VCH, New York, 1998.
- 7 C. Hardacre, J. D. Holbrey, C. L. Mullan, M. Nieuwenhuyzen, W. M. Reichert, K. R. Seddon and S. J. Teat, *New J. Chem.*, 2008, **32**, 1953.
- 8 J. C. Tiller, C. J. Liao, K. Lewis and A. M. Klibanov, *Proc. Natl. Acad. Sci. U. S. A.*, 2001, **98**, 5981.
- 9 (a) E. Alami, H. Levy, R. Zana, P. Weber and A. Skoulios, *Liq. Cryst.*, 1993, **13**, 201; (b) L. Lu, N. Sharma, G. A. N. Gowda, C. L. Khetrpal and R. G. Weiss, *Liq. Cryst.*, 1997, **22**, 23; (c) F. Tittarelli, P. Masson and A. Skoulios, *Liq. Cryst.*, 1997, **22**, 721; (d) M. Arkas, D. Tsiourvas, C. M. Paleos and A. Skoulios, *Chem. Eur. J.*, 1999, **5**, 3202; (e) R. Martin-Rapun, M. Marcos, A. Omenat, J. Barbera, P. Romero and J. L. Serrano, *J. Am. Chem. Soc.*, 2005, **127**, 7397; (f) M. Marcos, R. Martin-Rapun, A. Omenat, J. Barbera, P. Romero and J. L. Serrano, *Chem. Mater.*, 2006, **18**, 1206; (g) M. Marcos, R. Alcalá, J. Barbera, P. Romero, C. Sanchez and J. L. Serrano, *Chem. Mater.*, 2008, **20**, 5209; (h) Q. Zhang and C. G. Bazuin, *Macromolecules*, 2009, **42**, 4775.
- 10 (a) D. J. Abdallah, A. Robertson, H.-F. Hsu and R. G. Weiss, *J. Am. Chem. Soc.*, 2000, **122**, 3053; (b) H. Chen, D. C. Kwait, Z. S. Gonen, B. T. Weslowski, D. J. Abdallah and R. G. Weiss, *Chem. Mater.*, 2002, **14**, 4063; (c) K. F. Ma, B. S. Somashekhar, G. A. Nagana Gowda, C. L. Khetrpal and R. G. Weiss, *Langmuir*, 2008, **24**, 2746; (d) K. F. Ma, A. A. Shahkhatuni, B. S. Somashekhar, G. A. Nagana Gowda, Y. Y. Tong, C. L. Khetrpal and R. G. Weiss, *Langmuir*, 2008, **24**, 9843; (e) K. F. Ma, K. M. Lee, L. Minkova and R. G. Weiss, *J. Org. Chem.*, 2009, **74**, 2088.
- 11 (a) C. J. Bowles, D. W. Bruce and K. R. Seddon, *Chem. Commun.*, 1996, 1625; (b) C. M. Gordon, D. JohnHolbrey, A. R. Kennedy and K. R. Seddon, *J. Mater. Chem.*, 1998, **8**, 2627; (c) J. D. Holbrey and Seddon, *J. Chem. Soc., Dalton Trans.*, 1999, 2133; (d) A. E. Bradley, C. Hardacre, J. D. Holbrey, S. Johnston, S. E. J. McMath and M. Nieuwenhuyzen, *Chem. Mater.*, 2002, **14**, 629; (e) W. Dobbs, L. Douce, L. Allouche, A. Louati, F. Malbosc and R. Welter, *New J. Chem.*, 2006, **30**, 528; (f) P. H. J. Kouwer and T. M. Swager, *J. Am. Chem. Soc.*, 2007, **129**, 14042; (g) K. Goossens, P. Nockemann, K. Driesen, B. Goderis, C. Gorller-Walrand, K. V. Hecke, L. V. Meervelt, E. Pouzet, K. Binnemans and T. Cardinael, *Chem. Mater.*, 2008, **20**, 157; (h) V. Causin and G. Saielli, *J. Mater. Chem.*, 2009, **19**, 9153.
- 12 (a) K. Goossens, K. Lava, P. Nockemann, K. V. Hecke, L. V. Meervelt, K. Driesen, C. Gorller-Walrand, K. Binnemans and T. Cardinael, *Chem. Eur. J.*, 2009, **15**, 656; (b) K. Goossens, K. Lava, P. Nockemann, K. V. Hecke, L. V. Meervelt, P. Pattison, K. Binnemans and T. Cardinael, *Langmuir*, 2009, **25**, 5881.
- 13 (a) E. J. R. SudhoHer, J. B. F. N. Engberts and W. H. de Jeur, *J. Phys. Chem.*, 1982, **86**, 1908; (b) M. Tabrizian, A. Soldera, M. Couturier and C. G. Bazuin, *Liq. Cryst.*, 1995, **18**, 475; (c) Y. Haramoto, Y. Akiyama, R. Segawa, S. Ujiie and M. Nanasawa, *J. Mater. Chem.*, 1998, **8**, 275; (d) F. Neve, A. Crispini and S. Armentano, *Chem. Mater.*, 1998, **10**, 1904; (e) F. Neve, O. Francescangeli, A. Crispini and J. Charmant, *Chem. Mater.*, 2001, **13**, 2032; (f) C. Rocoboy, F. Hampel and J. A. Gladysz, *J. Org. Chem.*, 2002, **67**, 6863; (g) D. Haristov and D. Tsiourvas, *Chem. Mater.*, 2003, **15**, 2079; (h) F. L. Celso, I. Pibiri, A. Triolo, R. Triolo, A. Pace, S. Buscemib and N. Vivona, *J. Mater. Chem.*, 2007, **17**, 1201; (i) D. Ster, U. Baumeister, J. Lorenzo Chao, C. Tschierskea and G. Israel, *J. Mater. Chem.*, 2007, **17**, 3393.
- 14 (a) K. M. Lee, C. K. Lee and I. J. B. Lin, *Angew. Chem., Int. Ed. Engl.*, 1997, **36**, 1850; (b) K. M. Lee, C. K. Lee and I. J. B. Lin, *Chem. Commun.*, 1997, 899; (c) C. K. Lee, H. W. Huang and I. J. B. Lin, *Chem. Commun.*, 2000, 1911; (d) K. M. Lee, Y. T. Lee and I. J. B. Lin, *J. Mater. Chem.*, 2003, **13**, 1079; (e) C. K. Lee, H. H. Peng and I. J. B. Lin, *Chem. Mater.*, 2004, **16**, 530; (f) C. S. Vasam and I. J. B. Lin, *J. Organomet. Chem.*, 2005, **690**, 3498; (g) J. Y. Z. Chiou, J. N. Chen, J. S. Lei and I. J. B. Lin, *J. Mater. Chem.*, 2006, **16**, 2972; (h) S. J. Hsu, K. M. Hsu, Max K. Leong and I. J. B. Lin, *Dalton Trans.*, 2008, 1924; (i) T. W. RoyHuang, W. C. Wang, R. Y. Yang, J. T. Lu and I. J. B. Lin, *Dalton Trans.*, 2009, 7121.
- 15 (a) S. K. Freeman, W. F. Ringk and P. E. Spoerri, *J. Am. Chem. Soc.*, 1947, **69**, 858; (b) F. You and R. J. Twieg, *Tetrahedron Lett.*, 1999, **40**, 8759.
- 16 H. Skaff and T. Emrick, *Chem. Commun.*, 2003, 52.
- 17 (a) G. H. Schmid and A. W. Wolkoff, *Can. J. Chem.*, 1972, **50**, 1181; (b) H. C. Lin, J. M. Shiau, R. C. Liu, C. Tsai and H. H. Tso, *Liq. Cryst.*, 1998, **25**, 277; (c) H. C. Lin, J. M. Shiau, C. Y. Wu and C. Tsai, *Liq. Cryst.*, 2000, **27**, 1103.
- 18 (a) J. Wang and R. J. Boyd, *J. Phys. Chem.*, 1996, **100**, 16141; (b) A. V. Chuchuryukin, P. A. Chase, A. M. Mills, M. Lutz, A. L. Spek, G. P. M. van Klink and G. van Koten, *Inorg. Chem.*, 2006, **45**, 2045.
- 19 *Inorganic Chemistry: Principles of Structure and Reactivity* (Ed.: James E. Huheey, Ellen A. Keiter, Richard L. Keiter), HarperCollins, 2005.
- 20 (a) J. Crank, *The Mathematics of Diffusion*, 2nd ed., Claxendon Press, Oxford, 1975; (b) E. L. Cussler, *Diffusion: Mass Transfer in Fluid Systems*, Cambridge University Press, Cambridge, 1984.
- 21 M. Trilla, R. Pleixats, T. Parella, C. Blanc, P. Dieudonne, Y. Guari and M. W. C. Man, *Langmuir*, 2008, **24**, 259.
- 22 (a) M. A. El-Sayed, *Acc. Chem. Res.*, 2001, **34**, 257; (b) M. C. Daniel and D. Astruc, *Chem. Rev.*, 2004, **104**, 293.
- 23 (a) M. Brust, M. Walker, D. Bethell, D. J. Schiffrin and R. J. Whyman, *J. Chem. Soc., Chem. Commun.*, 1994, 801; (b) M. Brust, J. Fink, D. Bethell, D. J. Schiffrin and C. J. Kiely, *J. Chem. Soc., Chem. Commun.*, 1995, 1655; (c) A. C. Templeton, W. P. Wuefling and R. W. Murray, *Acc. Chem. Res.*, 2000, **33**, 27.
- 24 (a) W. W. Weare, S. M. Reed, M. G. Warner and J. E. Hutchison, *J. Am. Chem. Soc.*, 2000, **122**, 12890; (b) M. Yamamoto and M. Nakamoto, *Chem. Lett.*, 2003, **32**, 452.
- 25 (a) S. J. Hsu, K. M. Hsu, M. K. Leong and I. J. B. Lin, *Dalton Trans.*, 2008, 1924; (b) P. Dash and R. W. J. Scott, *Chem. Commun.*, 2009, 812.
- 26 (a) D. I. Gittins and F. Caruso, *Angew. Chem., Int. Ed.*, 2001, **40**, 3001; (b) V. J. Gandubert and R. B. Lennox, *Langmuir*, 2005, **21**, 6532; (c) S. Rucareanu, V. J. Gandubert and R. B. Lennox, *Chem. Mater.*, 2006, **18**, 4674; (d) K. B. Male, J. Li, C. C. Bun, S. C. Ng and J. H. T. Luong, *J. Phys. Chem. C*, 2008, **112**, 443.
- 27 (a) S. Singh, R. Pasricha, U. M. Bhatta, P. V. Satyam, M. Sastrya and B. L. V. Prasad, *J. Mater. Chem.*, 2007, **17**, 1614; (b) M. Conte, K. Wilson and V. Chechik, *Org. Biomol. Chem.*, 2009, **7**, 1361.
- 28 (a) M. M. Alvarez, J. T. Khoury, T. G. Schaaff, M. N. Shafigullin, I. Vezmar and R. L. Whetten, *J. Phys. Chem. B*, 1997, **101**, 3706; (b) A. Moores and F. Goettmann, *New J. Chem.*, 2006, **30**, 1121.